OPTICAL FIBRES AND FIBRE-OPTIC INSTRUMENTS

PACS numbers: 42.55.Wd; 42.81.Cn
DOI: 10.1070/QE2011v041n09ABEH014576

Effect of optical pumping on the refractive index and temperature in the core of active fibre

V.V. Gainov, O.A. Ryabushkin

Abstract. **This paper examines the refractive index change (RIC) induced in the core of Yb^{3+}-doped active silica fibres by pulsed pumping. RIC kinetic measurements with a Mach–Zehnder interferometer make it possible to separately assess the contributions of the electronic and thermal mechanisms to the RIC and evaluate temperature nonuniformities in the fibre.**

Keywords: *fibre laser, Mach–Zehnder interferometer, refractive index profile, cross-sectional temperature profile, polarisability difference.*

1. Introduction

High-power single-mode rare-earth-doped silica fibre lasers are widely used in materials processing [1]. The most widespread types of active fibres are few-mode (in particular, single-mode) fibres doped with Yb^{3+} (lasing in the spectral range 975–1100 nm) or with Er^{3+}, which ensures light amplification in the range 1535–1600 nm, with the addition of ytterbium ions for efficient photoexcitation at laser diode pump wavelengths (920–970 nm).

To couple in a pump beam, use is commonly made of so-called double-clad fibre designs, in which multimode pump light is absorbed in a rare-earth-doped guiding core. As a rule, such fibres have a step index profile (Fig. 1). To obtain high optical powers and reduce the threshold for nonlinear effects, most high-power fibre lasers employ few-mode fibre with a large fundamental mode diameter. Although the active ions are in general unevenly distributed over the core of such fibre [2], in modelling the properties of active fibres we will take the rare-earth ions to be evenly distributed over a cylinder of diameter d. The fibre core diameter is a. The overlap of the fundamental mode field and doped region will be characterised by a coefficient Γ_{core}.

Pump power absorption in an active medium is accompanied by heating of the fibre (so that cross-section spectra vary considerably with temperature [3, 4]) and changes in refractive index profile. The appreciable (10^{-4} to 10^{-3}) change in the index difference between the core (n_{core}) and cladding (n_{clad}) in high-power fibre lasers and amplifiers has a significant effect on the modal characteristics of the active fibre.

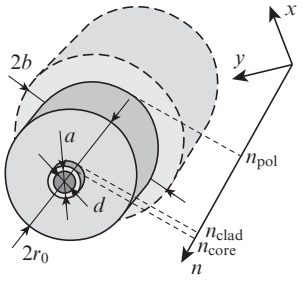

Figure 1. Schematic representation of the refractive index profile of an active fibre.

This paper examines the following two main mechanisms underlying optical pumping-induced refractive index changes (RICs):

(1) heating of the active fibre because of the difference between the pump and laser photon energies and through the absorption and scattering in the active medium [5, 6] and polymer coating, and

(2) change in the polarisation of the active medium in response to changes in laser level populations [7–9].

The temperature coefficient of the refractive index (thermo-optic coefficient) of silica glass is $\alpha_T = 10^{-5}$ K^{-1} [10]. The effect of cross-sectional temperature nonuniformity on the index profile of active fibres has been the subject of a detailed theoretical analysis [6]. As shown by numerical studies, the maximum permissible RIC value in the core of an active fibre determines the maximum heat power deposited per unit volume in the active medium. In the case of typical fibre geometries, the contribution of photoelastic effects can be neglected. For an ytterbium-doped fibre with a core diameter of 9.2 μm and a permissible RIC of 0.002, the limiting output power per unit fibre length was determined to be 2.9 kW cm^{-1}, which exceeds that for state-of-the-art high-power single-mode fibre lasers and amplifiers by almost three orders of magnitude [11, 12]. Nevertheless, it is of interest to experimentally study the effect of high-power optical pumping on the relative temperature nonuniformity in active fibre because the modal properties of few-mode active fibres with a large fundamental mode diameter (so-called large mode area fibres) are sensitive to even much lower index gradients [13].

Resonance light absorption by active ions changes the population of electronic levels and, accordingly, the polarisation of the active medium. This mechanism will be referred to as an electronic mechanism of RICs. It is convenient to describe

V.V. Gainov, O.A. Ryabushkin IRE-Polus Science and Technology Association, pl. Vvedenskogo 1, 141190 Fryazino, Moscow region, Russia; Moscow Institute of Physics and Technology (State University), Institutskii per. 9, 141700 Dolgoprudnyi, Moscow region, Russia; V.A. Kotel'nikov Institute of Radio Engineering and Electronics (Fryazino Branch), Russian Academy of Sciences, pl. Vvedenskogo 1, 141190 Fryazino, Moscow region, Russia; e-mail: vg254@rambler.ru, roa228@mail.ru

Received 28 February 2011; revision received 5 July 2011
Kvantovaya Elektronika **41** (9) 809–814 (2011)
Translated by O.M. Tsarev

the corresponding RIC, with allowance for the local field, using the Lorentz–Lorenz formula:

$$\frac{(n-\mathrm{i}\kappa)^2-1}{(n-\mathrm{i}\kappa)^2+2}=\frac{4\pi}{3}\sum_i p_i(\omega)N_i\,, \tag{1}$$

$$p_i(\omega)=\frac{e^2}{m_\mathrm{e}}\sum_j\frac{f_{ij}}{\omega_{ij}^2-\omega^2+\mathrm{i}\omega\Gamma_{ij}}\,, \tag{2}$$

where n is the real part of the refractive index; κ is the extinction coefficient; $p_i(\omega)$ is the polarisability of an atom (ion) in state i at frequency ω; N_i is the population of state i; ω_{ij}, Γ_{ij} and f_{ij} are, respectively, the frequency, attenuation coefficient and oscillator strength of the corresponding transition; and e and m_e are the electronic charge and mass. The oscillator strength is the ratio of the excited state relaxation rate, quantified by the Einstein coefficient A_{ij}, to the damping rate, γ_{ij}, of a classic oscillator of frequency ω_{ij} per degree of freedom:

$$|f_{ij}|=\frac{1}{3}\frac{A_{ij}}{\gamma_{ij}}=\frac{1}{\tau}\frac{m_\mathrm{e}c^3}{2\omega_{ij}^2e^2}\,, \tag{3}$$

where $\tau=1/A_{ij}$ is the excited state radiative lifetime. We have $f_{ij}<0$ for transitions with photon emission and $f_{ij}>0$ for transitions with photon absorption. Moreover,

$$f_{ij}=-\frac{g_j}{g_i}f_{ji}, \tag{4}$$

where g_i and g_j are the degeneracies of the levels involved [14].

For small increments of the real part of the refractive index, Eqn (4) can be written in the form

$$\Delta n=\frac{2\pi F_L^2}{n}\sum_i\Delta p_iN_i\,, \tag{5}$$

where $F_L=\frac{1}{3}(n^2+2)$ is the local field factor and Δp_i is the difference in polarisability between the ground and ith excited levels. If the populations of only the ground level and one metastable level undergo changes, (5) has only one term, proportional to N_2.

The electronic mechanism of RICs in both bulk solid lasing media and optical fibres has been investigated by many groups since the 1990s [8, 9, 15–22] (see also Ref. [7]). It is of interest to study this mechanism both in bulk solids, because electronic RICs influence laser beam parameters [9, 18, 20, 22], and in optical fibres, because resonance dispersion effects take place in erbium-doped fibre amplifiers under optical pumping [15, 19] and because electronic RICs are used in optical switching and coherent beam combining [7, 16, 17, 21]. Experiments with the use of different configurations of bulk and fibre interferometers, such as Mach–Zehnder, Michelson and twin-core fibre interferometers, made it possible to obtain RIC values, the oscillator strengths of the transitions involved and spectral dependences of the RIC.

According to data in the literature and expansion (2), the dominant contribution to RICs (in particular, near the resonance of the active ions) comes from dipole-allowed transitions with a short lifetime and, accordingly, with a larger oscillator strength in comparison with laser transitions. For the rare-earth ions in question in silica glass, these are electronic transitions in the UV spectral region to a $5d^1$ configuration:

$$\Delta p=\Delta p_{12}+\Delta p_{4f-5d},\quad \Delta p_{12}\ll\Delta p_{4f-5d}. \tag{6}$$

At present, approximation (6) is thought to be an established fact for the Yb^{3+} ion, but there are contradictory data for erbium-doped active media (cf. Refs [7] and [19]). Even though considerable effort has been concentrated on this area of research, no RIC measurements have been made under lasing conditions. Such measurements were the main purpose of this work. When the lasing threshold is reached, the population inversion takes a steady-state value, which enables the thermal contribution to the RIC to be directly assessed.

2. Experimental procedure and measurement results

In this work, we propose a temporal interferometric technique for RIC measurements in active fibres under luminescence and lasing conditions [23]. Using pulsed excitation of an active medium, one can separately assess the contributions of the various physical processes responsible for RICs and differing in rate. The experimental setup used is shown schematically in Fig. 2.

We performed measurements for Yb^{3+}-doped phosphosilicate glass fibres. The probe light source was a distributed-feedback (DFB) semiconductor laser with an emission wavelength $\lambda_\mathrm{s}=1564$ nm and an emission bandwidth of 2 MHz, corresponding to a coherence length of ~103 m. The probe wavelength, λ_s, was selected far away from the absorption bands of the rare-earth ion to avoid absorption and amplification in the active medium. To evaluate the contribution of electronic RICs, one should know the difference between the polarisabilities of the active ions at the wavelengths λ_laser and λ_s. Neglecting far-from-resonance oscillator damping, using Eqns (2)–(4) and taking an Yb^{3+} $^2F_{5/2}$ excited state lifetime in phosphosilicate glass fibres $\tau_1=1.5$ ms, we obtain $\Delta p|_{1.55\,\mu\mathrm{m}}=$

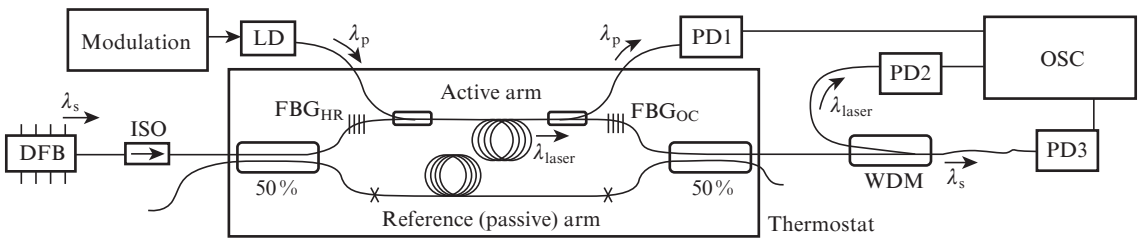

Figure 2. Schematic diagram of the experimental setup: LDs, pump diodes ($\lambda_\mathrm{p}=964$ nm); DFB, probe light laser source ($\lambda_\mathrm{s}=1564$ nm); ISO, optical isolator; PD1–PD3, photodetectors; $\mathrm{FBG_{HR}}$, highly reflective fibre Bragg grating; $\mathrm{FBG_{OC}}$, output fibre Bragg grating; WDM, wavelength division multiplexer; OSC, multichannel digital oscilloscope; $\lambda_\mathrm{laser}=1064$ nm, laser wavelength.

Table 1. Main parameters of the active arm.

Active fibre length/m	Yb^{3+} concentration/ppm	Core radius/μm	Pump wavelength/nm	Pump absorption coefficient/dB m^{-1}	$\Delta n/10^{-3}$	λ_{OC}/nm	R_{OC}/dB	$\Delta\lambda_{OC}$/nm
3	4200	5	964	1.2	14	1064	–4.31	0.42

Note: λ_{OC}, $\Delta\lambda_{OC}$, R_{OC} are the centre wavelength, bandwidth and reflectance of the output grating.

-1.1×10^{-27} cm^3. Note that the calculated polarisability difference at $\lambda = 1.5$ μm for the main ytterbium ion transition is an order of magnitude smaller in absolute value than that obtained by Fotiadi et al. [21] using a similar, noncavity interferometric technique. This lends support to a model relying on assumption (6). We also measured Δp in ytterbium-doped fibres at 1564 nm.

Parameters of the active arm in our experimental setup (Fig. 2) are listed in Table 1.

The laser diode pump power was amplitude-modulated by rectangular voltage pulses. The pump pulse rise time was 3 μs. We simultaneously recorded the signals of three photodetectors, which detected the pump light (PD1), interference signal (PD3) and laser output (PD2) in the active arm. Figure 3 illustrates the kinetics of the variation in the phase (phase difference, $\Delta\varphi$) of the probe light.

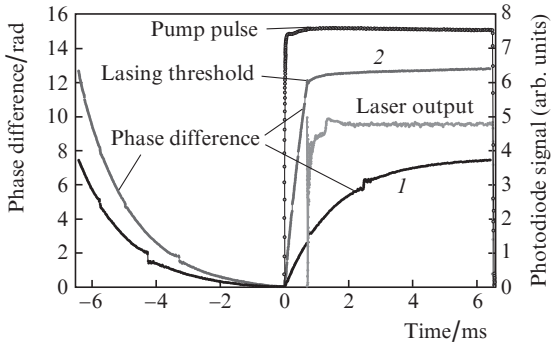

Figure 3. Time variation of the phase difference for meander-shaped pump pulses.

The phase difference curves in Fig. 3 are for pump powers of 0.3 (*1*) and 1.22 W (*2*). The well-defined break in curve (*2*) corresponds to the lasing threshold. Its exact position on the time scale can be determined from an oscilloscope trace of the laser output. The small discontinuities in the phase difference curves below threshold are due to changes in the visibility of the interference pattern. The results of more detailed phase difference measurements for ytterbium-doped fibres are presented in Fig. 4 (solid lines).

Figure 4a shows a well-defined break at pump powers above threshold, corresponding to the onset of lasing in the ytterbium-doped fibre. Above the lasing threshold, the active medium has a constant population inversion, but $\Delta\varphi$ increases further because of the rise in the temperature of the core of the active fibre (Fig. 4b). The kinetics of the variation in phase difference after switching off the pump power are governed not only by the spontaneous decay and reduction in metastable level population but also by the relaxation of the cross-sectional temperature profile.

As seen in Fig. 4a, even at pump powers three times above threshold for the ytterbium-doped fibre, the increase in phase difference after the lasing threshold is reached is insignificant

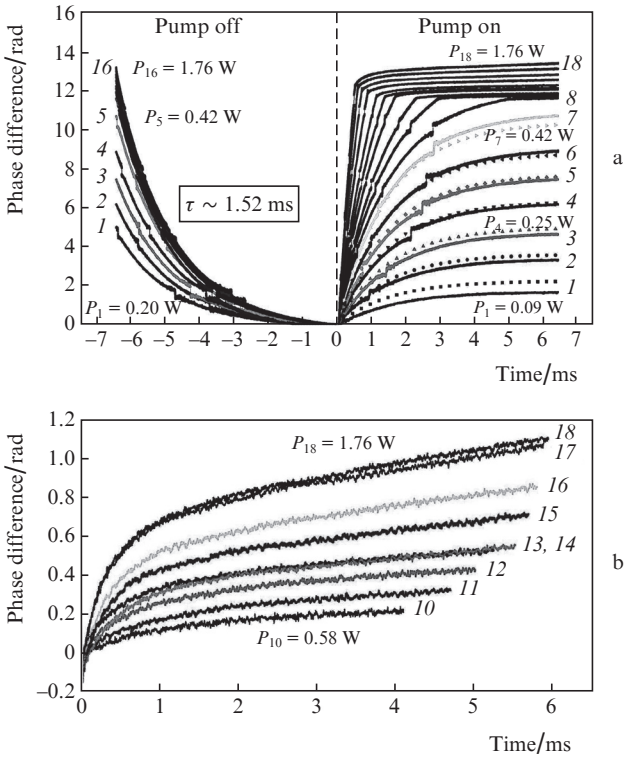

Figure 4. Time variation of the phase difference at different pump powers: (a) pump off/on, (b) above lasing threshold. Time zero in panel b corresponds to the onset of lasing.

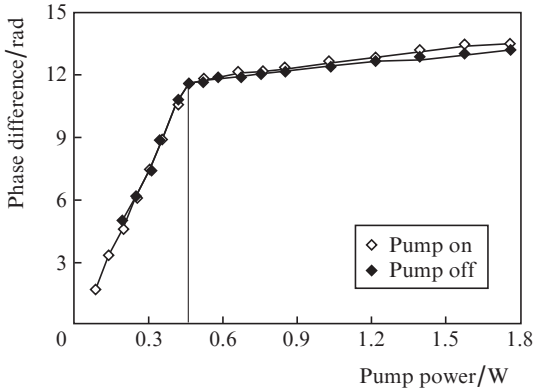

Figure 5. Total phase difference over a pump pulse as a function of pump power for Yb^{3+}-doped fibre. The vertical line represents the lasing threshold.

compared to that below threshold. Figure 5 plots the total phase difference against pump power.

3. Analysis of the results

The large difference in slope below and above the lasing threshold in Fig. 5 indicates that the variation in phase difference below threshold is mainly due to the electronic mechanism.

According to expansion (5), the time variation of the phase difference can be represented in the form

$$\Delta\varphi(t) = \frac{4\pi^2 F_L^2}{n\lambda_s}\Delta p(\lambda_s)\Gamma_{core}\int_0^L N_2(z,t)\mathrm{d}z, \quad (7)$$

where L is the length of the active fibre.

The active scheme under examination has a sufficiently low threshold gain, and this allows us to neglect the influence of amplified spontaneous emission on the metastable level population, N_2, as supported by the essentially linear variation of the total phase difference with pump power below the lasing threshold (Fig. 5). In addition, we take that the population inversion changes only slightly during the time needed for a pump pulse to pass through the active medium. With these assumptions, the system of rate equations below threshold has the form

$$\begin{cases}\dfrac{\partial N_2}{\partial t} = \dfrac{I}{h\nu}[\sigma_{ab}N_{Yb} - (\sigma_{ab}+\sigma_{em})N_2] - \dfrac{N_2}{\tau_1},\\ \dfrac{\partial I}{\partial z} = \Gamma_p I[(\sigma_{ab}+\sigma_{em})N_2 - \sigma_{ab}N_{Yb}],\end{cases} \quad (8)$$

where $\Gamma_p = A_{core}/A_{clad}$ is the overlap coefficient for the multimode pump field and doped core; I and $h\nu$ are the pump intensity and pump photon energy; σ_{ab} and σ_{em} are the absorption and emission cross sections; N_{Yb} is the Yb^{3+} concentration; and z is a longitudinal coordinate.

In active media with an Yb^{3+} concentration $N_{Yb} = 4200$ ppm, the threshold upper level population is under 5%, so the pump intensity can be thought to be steady-state and exponentially decrease along the active fibre with an attenuation coefficient $\alpha_p = -\Gamma_p\sigma_{ab}N_{Yb}$. Then, we obtain from the former equation in (8)

$$N_2(z,t) = \frac{I(z)}{I_{sat}[1+I(z)/I_{sat}](1+\xi)} \times\left\{1-\exp\left[-\frac{t}{\tau_1}\left(1+\frac{I(z)}{I_{sat}}\right)\right]\right\}, \quad (9)$$

where $\xi = \sigma_{em}/\sigma_{ab}$ and $I_{sat} = h\nu/[(\sigma_{ab}+\sigma_{em})\tau_1]$ is the saturation intensity at the pump wavelength. At the end of a pump pulse, the upper level population reaches a steady-state value and the second term in (9) can be neglected. Substituting the expression for the steady-state population into (7) and integrating over the fibre length, we obtain in the $I \ll I_{sat}$ approximation

$$\Delta\varphi_{sum} = \delta\Delta pP, \quad (10)$$

$$\delta = \frac{4\pi^2 F_L^2}{n\lambda_s}\frac{\Gamma_{core}N_{Yb}[1-\exp(-\alpha_p L)]}{A_{clad}\alpha_p I_{sat}(1+\xi)}, \quad (11)$$

where P is the input pump power.

The sought polarisability difference can be found if one knows the slope of the left part of the plot in Fig. 5, which is 27.2 ± 0.4 rad W^{-1}. The error of determination is here also contributed by the quantities that appear in the expression for δ [Eqn (11)]. The largest uncertainty comes from the overlap coefficient Γ_{core}, which is evaluated by numerically calculating the fundamental mode profile from preset refractive index profile parameters (with allowance for the measurement accuracy). The active fibre under examination has $\Gamma_{core} = 0.64–0.70$, which corresponds to a relative uncertainty of about 10%. The other parameters of the fibre, $N_{Yb} = 4200$ ppm $= 2.7\times10^{26}$ m^{-3}, $A_{clad}I_{sat} = 7.3$ W and $\xi = 0.66$, are accurate to within 5%. From these data, the estimated Yb^{3+} polarisability difference in phosphosilicate glass fibres at 1.55 μm is $\Delta p = (2.6\pm0.4)\times10^{-26}$ cm^3.

This value differs significantly from that reported by Fotiadi et al. [21], which may be due to the influence of the field of neighbouring ions on the spectroscopic characteristics of laser transitions and transitions from the outermost electron shells of rare-earth elements in silica glass (Fotiadi et al. [21] studied aluminosilicate glass fibres).

Integrating Eqns (8) with respect to time by the fourth-order Runge–Kutta method for each z value, we find the phase difference as a function of time below the lasing threshold (Fig. 4a). The $\Delta\varphi(t)$ curves calculated for the polarisability difference Δp found above are represented in Fig. 4a by points.

The kinetics of the variation in phase difference above the lasing threshold in Fig. 4b are well fitted with functions of the form

$$\varphi(t) = A_T[1-\exp(-1/\tau_T)] + \beta t + \beta_0, \quad (12)$$

where the first term represents the evolution of the cross-sectional temperature profile in the fibre. Figure 6 plots the amplitude factor A_T and thermal relaxation time τ_T against pump power.

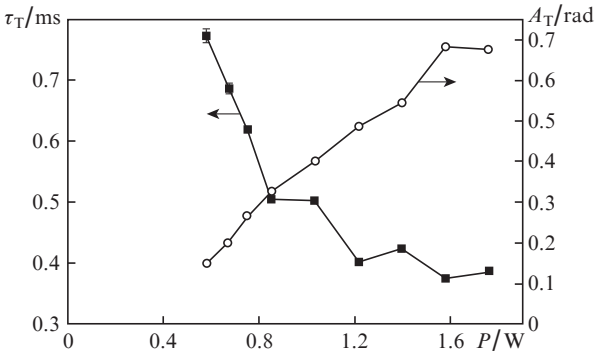

Figure 6. Amplitude factor A_T and thermal relaxation time τ_T as functions of pump power.

The amplitude A_T in Eqn (12) can be related to the fibre-length-averaged core–cladding temperature difference, ΔT_{core}:

$$A_T = \frac{2\pi}{\lambda_s}nL\alpha_T\Delta T_{core}. \quad (13)$$

At a slope $\Delta A_T/\Delta P = 0.46$ rad W^{-1} (Fig. 6), we have $\Delta T_{core}/\Delta P = 0.38\times10^{-2}$ K W^{-1}.

To verify the proposed model, we evaluated the heating of an active fibre by numerically solving an unsteady-state heat equation for an axisymmetric geometry (Fig. 1): a silica fibre of radius r_0, with a core of diameter d, doped with active ions, and a polymer cladding of outer diameter $2b$. The heat equation for this system has the form

$$k\frac{1}{r}\frac{\partial}{\partial r}r\frac{\partial\Delta T}{\partial r} + Q = \rho c_v\frac{\partial\Delta T}{\partial t}, \quad (14)$$

where k is the thermal conductivity of the corresponding layer (k_1 for silica glass and k_2 for the polymer cladding); ρ is density; c_v is specific heat capacity; $Q = \eta P_{ab}$ is the heat power deposited per unit volume; P_{ab} is the pump power absorbed per unit volume; and η is the fraction of absorbed pump power converted to heat.

As boundary conditions, we use the temperature and heat flux continuity constraints at the interfaces in the fibre and the convective heat transfer constraint on the outer side of the polymer cladding, characterised by a parameter h^T:

$$k_2 \frac{\partial \Delta T}{\partial r}\Big|_b = -h^T \Delta T(b). \quad (15)$$

Equation (14) was solved by the finite-difference method. The equation was discretised on a two-dimensional network using a three-point implicit scheme, and the system of linear equations obtained was solved by a sweep method. It should be emphasised that, in calculating the variation in phase difference, one should take into account the overlap of the fundamental mode intensity profile and temperature profile in conformity with perturbation theory corrections [24]. Given that the absorbed pump power is an exponential function of longitudinal coordinate z, the phase difference can be represented in the form

$$\Delta\varphi(t) = \frac{2\pi n}{\lambda_s} \frac{\alpha_T[1 - \exp(-\alpha_p L)]}{\alpha_p} \frac{\int \Delta T(t,r)\psi^2(r)\,dr}{\int \psi^2(r)\,dr}, \quad (16)$$

where r is the radius; $\psi(r)$ is the normalised scalar amplitude of the fundamental mode field; and $\Delta T(t,r)$ is the cross-sectional temperature profile in the fibre at a given input pump power. In both the numerator and denominator in Eqn (16), the integration is performed over the cross section of the fibre.

In our calculations, the following parameters were used: $k_1 = 1.46$ W m^{-1} K^{-1}, $k_2 = 0.2$ W m^{-1} K^{-1}, $d = 10$ μm, $r_0 = 62.5$ μm, $b = 182$ μm, $\eta = 0.09$, $h^T = 25$ W m^{-2} K^{-1}, $\rho c_v|_1 = 2.14\times10^6$ J m^{-3} K^{-1} and $\rho c_v|_2 = 1.33\times10^6$ J m^{-3} K^{-1} [25] (Sylgard® 182 polymer).

Figure 7 shows the time dependences of the temperature change in the fibre core and cladding and the difference curve for a 1.55-W pump pulse, which corresponds to curve (*17*) in Fig. 4b. It follows from these data that the temperatures of the core and silica cladding increase during the first 10 ms, whereas the temperature of the polymer remains unchanged. This allows one to distinguish the heating of the core from that of the cladding in interference measurements in this time range. During the first few seconds or longer times, the fibre is slowly heated owing to the relatively weak convective heat transfer at the interface between the polymer and air (or another ambient medium). As can be seen in Fig. 7, the temperature nonuniformity is then two orders of magnitude less than the steady-state temperature. The steady-state temperature is reached at a rate considerably slower than the rates of electronic RICs and core heating, which allows this temperature to be measured. Such measurements were described in detail elsewhere [26].

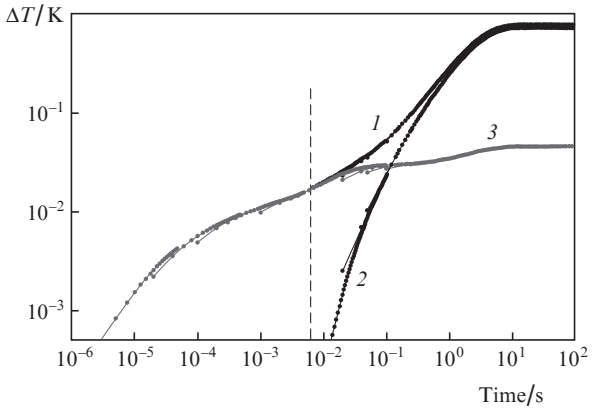

Figure 7. Time dependences of the temperature change (*1*) on the axis of the fibre core and (*2*) on the outer side of the polymer cladding after switching on 1.55-W pumping; (*3*) difference curve. The dashed line represents the end of the pump pulse in the experiment.

We compared the calculated phase change due to core heating with that measured after reaching the lasing threshold. Figure 8 shows the calculated curve and experimental data [Fig. 4b, curve (*17*)] for $P = 1.55$ W. As seen, the model gives a larger phase difference (and, accordingly, a higher temperature) in comparison with the measurement results. The reason for this is that some of the excited atoms experience deexcitation through spontaneous transitions, which considerably reduces the quantum energy defect. In the case of Yb^{3+} in phosphosilicate glass fibres, the effective quantum energy defect for spontaneous transitions, η_{sp}^{eff}, at the pump wavelength in question is 0.038 [25]. An exact model should take into account the inversion and laser intensity distributions along the length of the active fibre. Nevertheless, approximate calculations provide adequate order-of-magnitude estimates of core heating at a given pump power.

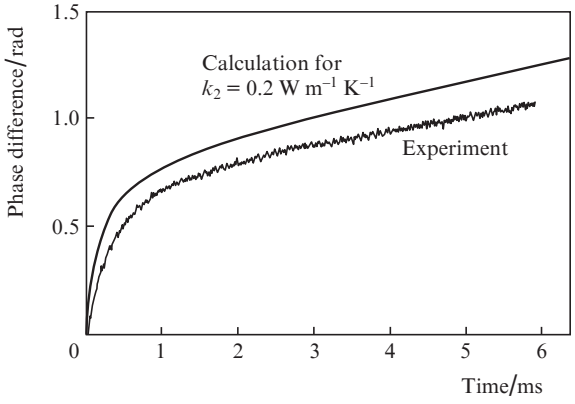

Figure 8. Comparison of the calculated and experimental phase differences as functions of time.

To compare the contributions of different physical processes to the total changes in the temperature and refractive index of Yb^{3+}-doped fibres, the measurement results are summarised in Table 2.

The first line gives the temperature change per watt of pump power, and the second line gives the corresponding RIC. The first column indicates the core–cladding temperature difference assessed from the time variation of the phase difference above the lasing threshold (Fig. 6), and the second column gives RIC values for the electronic mechanism, related to changes in the population of metastable levels of the active ion. In ytterbium-doped fibres, such RICs occur only below the lasing threshold. The third and fourth columns indicate the

Table 2. Changes in the refractive index and temperature of Yb^{3+}-doped fibre due to different physical processes.

	Thermal (heating of the core relative to the cladding)	Electronic (polarisability difference)	Thermal (steady-state heating of the fibre in a fibre block)	Thermal (steady-state heating of the fibre through air heat exchange)
$\Delta T/\Delta P$/K W^{-1}	0.38×10^{-2}		2.2	0.7
$\Delta n/\Delta P$/W^{-1}	0.38×10^{-7}	3.3×10^{-6}	2.2×10^{-5}	0.7×10^{-5}

temperature increment and RIC under thermal equilibrium conditions and different heat removal conditions: the active fibre is either in a protective, heat-removing polymer layer of a fibre block or in air under natural convection. The data were obtained earlier by steady-state measurements [26]. It can be seen from Table 2 that the steady-state temperature in the fibre exceeds the cross-sectional temperature nonuniformity by about two orders of magnitude, which qualitatively supports the heating model represented in Fig. 7.

4. Conclusions

We have measured the RIC induced in the core of Yb^{3+}-doped active phosphosilicate glass fibres by pulsed optical pumping and developed a kinetic measurement technique which allows the contributions of the electronic and thermal mechanisms to the resultant RIC to be separately assessed. The relative heating of the fibre core under lasing conditions has been experimentally determined for the first time and compared to the absolute value of the temperature. The present experimental data allow one to evaluate changes induced in the refractive index profile of optical fibres by high pump powers.

Acknowledgements. We are grateful to R. Shaidullin, a postgraduate at the Department of Photonics, Moscow Institute of Physics and Technology, for his assistance with this study.

References

1. Dianov E.M. *Kvantovaya Elektron.*, **40**, 1 (2010) [*Quantum Electron.*, **40**, 1 (2010)].
2. Hotoleanu M., Söderlund M., Kliner D., et al. *Proc. SPIE–Int. Soc. Opt. Eng.*, **6102**, 61021T (2006).
3. Brilliant N.A., Lagonik K. *Opt. Lett.*, **26**, 1669 (2001).
4. Grukh D.A., Kurkov A.S., Paramonov V.M., Dianov E.M. *Kvantovaya Elektron.*, **34**, 1 (2004) [*Quantum Electron.*, **34**, 1 (2004)].
5. Davis M.K., Digonnet M.J.F., Pantell R.H. *J. Lightwave Technol.*, **16**, 1013 (1998).
6. Brown D.C., Hoffman H.J. *IEEE J. Quantum Electron.*, **37**, 207 (2001).
7. Digonnet M.J.F., Sadowski R.W., Shaw H.J., Pantell R.H. *Opt. Fiber Technol.*, **3**, 44 (1997).
8. Butylkin V.S., Kaplan A.E., Khronopulo Yu.G., Yakubovich E.I. *Resonant Nonlinear Interactions of Light with Matter* (Berlin: Springer, 1977; Moscow: Nauka, 1977).
9. Antipov O.L., Kuzhelev A.S., Luk'yanov A.Yu., Zinov'ev A.P. *Kvantovaya Elektron.*, **25**, 891 (1998) [*Quantum Electron.*, **28**, 867 (1998)].
10. Kikoin I.K. (Ed.) *Tablitsy fizicheskikh velichin. Spravochnik* (Tables of Physical Quantities: A Handbook) (Moscow: Atomizdat, 1976).
11. Fomin V., Abramov M., Ferin A., et al. *Proc. 14th Int. Conf. on Laser Opt. «LO-2010»* (St. Petersburg, 2010) paper TuSy-1.3, p. 103.
12. Jeong Y., Yoo S., Codemard C.A., Nilsson J., et al. *IEEE J. Sel. Top. Quantum Electron.*, **13**, 573 (2007).
13. Bagett J.C., Monro T.M., Furusawa K., Richardson D.J. *Opt. Lett.*, **26**, 1045 (2001).
14. El'yashevich M.A. *Atomnaya i molekulyarnaya spektroskopiya* (Atomic and Molecular Spectroscopy) (Moscow: Editorial URSS, 2001).
15. Fleming S.C., Whitley T.J. *Electron. Lett.*, **27**, 1959 (1991).
16. Arkwright J.W., Elango P., Whitbread T.W., Atkins G.R. *IEEE Photonics Technol. Lett.*, **8**, 408 (1996).
17. Digonnet M.J.F., Sadowski R.W., Shaw H.J., Pantell R.H. *J. Lightwave Technol.*, **15**, 299 (1997).
18. Andrade A.A., Tenório E., Catunda T., et al. *J. Opt. Soc. Am. B*, **16**, 395 (1999).
19. Barmenkov Yu.O., Kir'yanov A.V., Andres M.V. *Appl. Phys. Lett.*, **85**, 2466 (2004).
20. Antipov O.L., Bredikhin D.V., Eremeikin O.N., et al. *Kvantovaya Elektron.*, **36**, 418 (2006) [*Quantum Electron.*, **36**, 418 (2006)].
21. Fotiadi A., Antipov O., Megret P. *Opt. Express*, **16**, 12658 (2008).
22. Antipov O.L., Anashkina E.A., Fedorova K.A. *Kvantovaya Elektron.*, **39**, 1131 (2009) [*Quantum Electron.*, **39**, 1131 (2009)].
23. Gainov V., Ryabushkin O.A. *Proc. 3rd EPS-QEOD Europhoton Conf.* (Paris, 2008) paper THoD.5.
24. Agrawal G.P. *Nonlinear Fiber Optics* (San Diego: Academic, 1995; Moscow: Mir, 1996).
25. Reinert F., Luthy W. *Opt. Express*, **13**, 10749 (2005).
26. Gainov V.V., Shaidullin R.I., Ryabushkin O.A. *Kvantovaya Elektron.*, **41**, 637 (2011) [*Quantum Electron.*, **41**, 637 (2011)].